The Permanent Electric Dipole Moments and Magnetic g_e-Factors of Praseodymium Monoxide (PrO)†

Hailing Wang,‡ Colan Linton,§ Tongmei Ma,|| and Timothy C. Steimle*,‡

Department of Chemistry and Biochemistry, Arizona State University, Tempe, Arizona 85287-1604, Centre for Laser Atomic and Molecular Sciences and Physics Department, University of New Brunswick, P.O. Box 4400, Fredericton, New Brunswick, Canada E3B 5A3, Department of Chemistry, South China University of Technology, Guangzhou, China

Received: January 22, 2009; Revised Manuscript Received: March 10, 2009

The $R(4.5)$ and $P(6.5)$ branch features of the XX (0, 0) band of praseodymium monoxide (PrO) have been studied at a resolution of approximately 50 MHz field free and in the presence of static electric and magnetic fields. The permanent electric dipole moments, μ_{el}, of 3.01(6) D and 4.72(5) D for the X_2 ($\Omega = 4.5$) and [18.1] ($\Omega = 5.5$) states, respectively, were determined from the analysis of the Stark spectra. The magnetic g_e-factors of 4.48(8) and 5.73(6) for the X_2 ($\Omega = 4.5$) and [18.1] ($\Omega = 5.5$) states, respectively, were determined from the analysis of the Zeeman spectra. The g_e-factors are compared with those computed using wave functions predicted from ligand field theory and ab initio calculations. The μ_{el} value for the X_2 ($\Omega = 4.5$) state is compared to ab initio and density functional predicted values and with the experimental values of other lanthanide monoxides.

Introduction

The very complex optical spectra of the lanthanide monoxides are caused by the insensitivity of the electronic energies to the numerous possible arrangements of the Ln^{2+} electrons in the 4f and 6s orbitals. Fortunately, the insensitivity of the electronic energies to the various occupations of the Ln^{2+} 4f and 6s orbitals also implies that disentangling the complex optical spectra may be aided by using simple ligand field theory (LFT) to establish the global electronic structure for the low-lying electronic states. Assessment of LFT, as well as more sophisticated electronic structure methodologies, is best achieved by comparing predicted magnetic hyperfine parameters, permanent electric dipole moments, μ_{el}, and magnetic dipole moment, μ_m, with experimentally measured values because all three properties are sensitive to the various arrangements of the Ln^{2+} 4f and 6s electrons. The limited number of valence electrons and the presence of a single isotopologue with nonzero nuclear spin makes praseodymium monoxide, $^{141}Pr(I = 5/2)O$, a favorable case among the lanthanide monoxide molecules for testing the predictability of LFT and other methodologies. Indeed, the interpretation of the magnetic hyperfine structure in the Doppler-limited laser induced fluorescence (LIF) spectra of PrO, which has been extensively studied by the Field group,[1−4] was instrumental in the original development of LFT for the lanthanide monoxides.[4−8] The magnetic hyperfine structure of the X_2 ($\Omega = 4.5$) ($E = 220$ cm^{-1}) and X_1 ($\Omega = 3.5$) ($E = 0$ cm^{-1}) states was also precisely characterized from the analysis of the laser-rf double resonance spectrum and interpreted using LFT.[9] Here, we report on the experimental determination of μ_{el} and μ_m for the X_2 ($\Omega = 4.5$) and [18.1] ($\Omega = 5.5$) states from the analysis of optical Stark and Zeeman spectra for the R(4.5) and P(6.5) lines of the XX (0, 0) band system. The XX (0, 0) band system is the transition between the ($v = 0$) [18.1] ($\Omega = 5.5$) and ($v = 0$) $X_2(\Omega = 4.5)$ vibronic levels. The results will be compared with values predicted from both LFT and ab initio electronic structure calculations. The small hyperfine splitting in the X_1 ($\Omega'' = 3.5$) ($E = 0$ cm^{-1}) precluded an analysis of Stark and Zeeman effect in the [16.6] ($\Omega' = 3.5$)−X_1 ($\Omega'' = 3.5$) ($E = 0$ cm^{-1}) (XVII (0, 0)) band, which was the initial objective of the present study.

The magnetic dipole moment of a nonrotating molecule results from a combination of the electronic orbital and electronic spin magnetic dipole moments of the individual electrons. The quantum mechanical operator for the individual electronic orbital and spin magnetic dipole moments are proportional to the individual orbital and spin angular momentum operators, $\hat{\mathbf{l}}$ and $\hat{\mathbf{s}}$, respectively. The proportionality constants are simply the Bohr magneton times either the electronic orbital g-factor (g_l) (= 1) or the spin g-factor (g_s) (= 2.0023). Thus, μ_m can be predicted a priori, given the molecular configurations of a particular electronic state, and conversely, any proposed molecular configuration for a given electronic state must be consistent with an experimentally measured μ_m.

Unlike μ_m, μ_{el} cannot be predicted a priori given a molecular configuration. The permanent electric dipole moment is particularly sensitive to the nature of the chemically relevant valence electrons and is used in the description of numerous phenomena. Accordingly, μ_{el} is routinely predicted from electronic structure calculations either as the expectation value of the dipole moment operator or from analysis of the finite electric field dependence of the energies. The comparison between the expectation value and finite field value is a primary diagnostic of the treatment of configuration interaction. Some time ago, a ground state μ_{el} value of 3.86 D was predicted by a self-consistent field/configuration interactions ab initio calculation using a pseudopotential for the 4f orbitals.[10] A recent density functional theory calculation implementing the B3LYP hybrid functionals predicts a ground state μ_{el} of 4.114 D.[11] The

† Part of the "Robert W. Field Festschrift".

* To whom correspondence should be addressed. Phone: (480) 965-3265. E-mail: Tsteimle@ASU.edu.

‡ Arizona State University.

§ University of New Brunswick.

|| South China University of Technology.

10.1021/jp900677g CCC: $40.75
Published on Web 04/20/2009

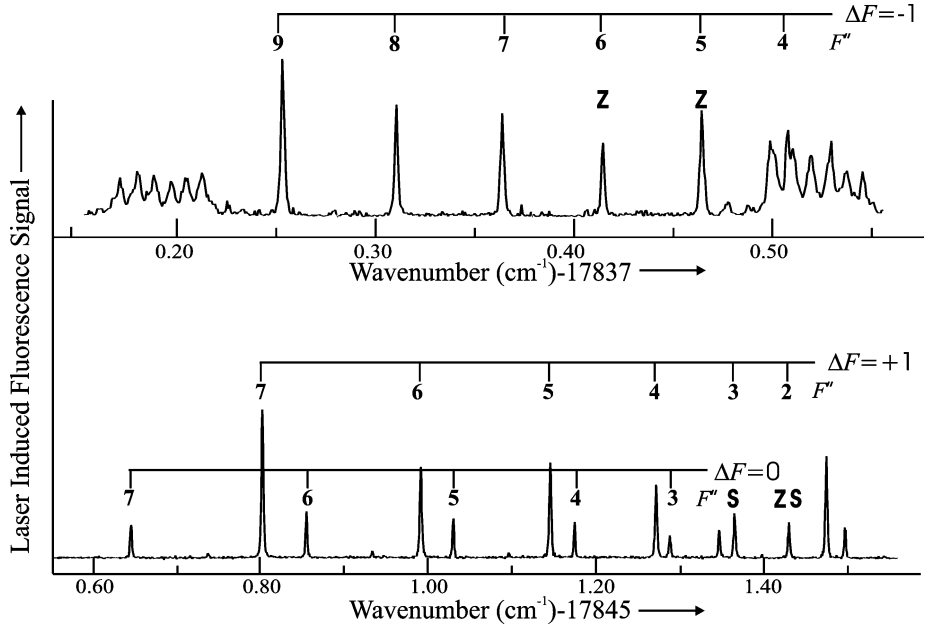

Figure 1. The field-free spectra of the $P(4.5)$ (top) and R (4.5) (bottom) branch feature of the XX (0, 0) band of the supersonic molecular beam sample of PrO. The splitting is due to the Pr($I = 9/2$) hyperfine interaction. The "S" and "Z" labels identify the transitions studied using optical Stark and Zeeman spectroscopy. The hyperfine multiplets at approximately 17 837.18 and 17 837.53 cm^{-1} belong to the $Q(28.5)$ and $Q(27.5)$ transitions, respectively.

semiempirical valence-electron calculation performed some time ago[12] determined the electronic state distribution and wave functions but did not predict μ_{el}. The two predicted values of μ_{el} are inconsistent with the experimentally determined trend of μ_{el} for the LnO series. Specifically, the experimentally determined ground state μ_{el} values for LaO (3.207 D),[13] CeO (3.119D) (see accompanying article), NdO (3.369D),[14] SmO (3.52 D),[15] DyO (4.51 D),[16] HoO (4.80 D),[17] and YbO (5.89 D)[18] exhibit a smooth variation with atomic number. Extrapolation of these values yields a dipole moment of approximately 3.2 D for PrO.

I. Experimental

The supersonic molecular beam spectrometer and the LIF optical detection scheme have been described previously.[19,20] A praseodymium rod was ablated by using the second harmonic (532 nm) of a Q-switched, pulsed Nd:YAG laser. The ablation products were entrained in a free-jet expansion of argon carrier gas seeded with ~10% oxygen with a backing pressure of 2000 kPa. The supersonic free-jet expansion was skimmed to produce a well-collimated molecular beam in a differentially pumped molecular beam machine. The XX (0, 0) band system fluorescence was detected off-resonance at 630 nm through a ±10 nm bandpass filter. The filtered LIF signal was detected by a cooled photomultipliter tube and processed using a gated single-photon counting technique. The spectral line widths of <50 MHz full width at half-maximum (fwhm) were achieved by the combination of molecular beam collimation and low laser intensity.

The static electric fields were obtained by applying a voltage across two partially transmitting neutral-density filters that straddled the region of molecular fluorescence. The field strength was calibrated using a voltmeter and physical measurement of the Stark plate spacing, yielding an estimated systematic error of 2%. The static magnetic fields were generated by using a homemade electromagnet. It consisted of a pair of Helmholtz coils with ferromagnetic poles through which 5 mm holes were drilled to allow for the passage of the molecular beam. The field was calibrated by a commercial Gauss meter. A systematic error of 2% was estimated for the magnetic field strength determination. A polarization rotator and polarizing filter were used to orient the electric field vector of the linearly polarized laser radiation either parallel, "∥", or perpendicular, "⊥", to that of the applied electric or magnetic field. These geometries result in transitions that obey the $\Delta M_F = 0$ (∥) or $\Delta M_F = \pm 1$ (⊥) selection rules, respectively, where M_F is the projection of F (the total angular momentum) along the field direction.

The Stark and Zeeman induced shifts and splittings were accurately measured by simultaneously recording the transmission of two confocal etalons. One etalon was actively stabilized and calibrated to have a free spectral range of 749.14 MHz. A second, unstabilized etalon with a free spectral range of 75.7 MHz was used to interpolate between transmission peaks of the stabilized etalon. The absolute wavenumbers were determined to an accuracy of ±0.0001 cm^{-1} by simultaneously recording the sub-Doppler I_2 absorption spectrum.[21,22] The measured transition wavenumbers agreed with those given in ref 2.

II. Observations

a. Field Free. The field free spectra for the $R(4.5)$ and $P(6.5)$ branch features are given in Figure 1. The intense $\Delta F = \Delta J$ transitions previously detected in the Doppler-limited LIF measurements[2] as well as the $\Delta F = \Delta J - 1$ transitions are readily assigned for the $R(4.5)$ line. A precise measure of the hyperfine splitting in the rotational levels associated with the $R(4.5)$ and $P(6.5)$ branch features of the XX (0, 0) band is required to account for second order effects in the analysis of the Zeeman and Stark spectra. The hyperfine energy level pattern in the X_2 ($\Omega = 4.5$) ($E = 220$ cm^{-1}) state exhibits a strong J-dependence because of rotational and hyperfine induced mixing with the X_1 ($\Omega'' = 3.5$) ($E = 0$ cm^{-1}) state. Specifically, the hyperfine splitting in the X_2 ($\Omega = 4.5$) ($E = 220$ cm^{-1}) is large at low J and rapidly decreases with increasing rotation, whereas splitting in the X_1 ($\Omega'' = 3.5$) ($E = 0$ cm^{-1}) is small at low J and rapidly increases.[4,9] The splittings between the adjacent energy levels within the hyperfine components of the

TABLE 1: Splitting of the F and F + 1 Hyperfine Levels in the Low-*J* Lines of the X_2 ($\Omega = 4.5$) and [18.1] ($\Omega = 5.5$) States

X_2 ($\Omega = 4.5$)				[18.1] ($\Omega = 5.5$)			
J	*F*	obs (cm^{-1})	dif[a] (cm^{-1})	*J*	*F*	obs (cm^{-1})	dif[a] (cm^{-1})
4.5	6	0.3599	0.0031	5.5	7	0.1633	–0.0003
	5	0.3061	0.0002		6	0.1442	0.0010
	4	0.2520	–0.0029		5	0.1220	–0.0007
	3	0.2033	–0.0006		4	0.1010	–0.0013
	2	0.1510	–0.0019		3	0.0833	0.0015
6.5	8	0.2236	–0.0015				
	7	0.2008	0.0008				
	6	0.1760	0.0010				
	5	0.1501	0.0001				

[a] Difference between the observed and calculated expectation value of $a_J\hat{I}\cdot\hat{J}$ in a Hund's case c_β basis set with $a_J = 0.0510$ cm^{-1}, 0.0205 cm^{-1}, and 0.0250 cm^{-1} for $J = 4.5$, 5.5, and 6.5, respectively.

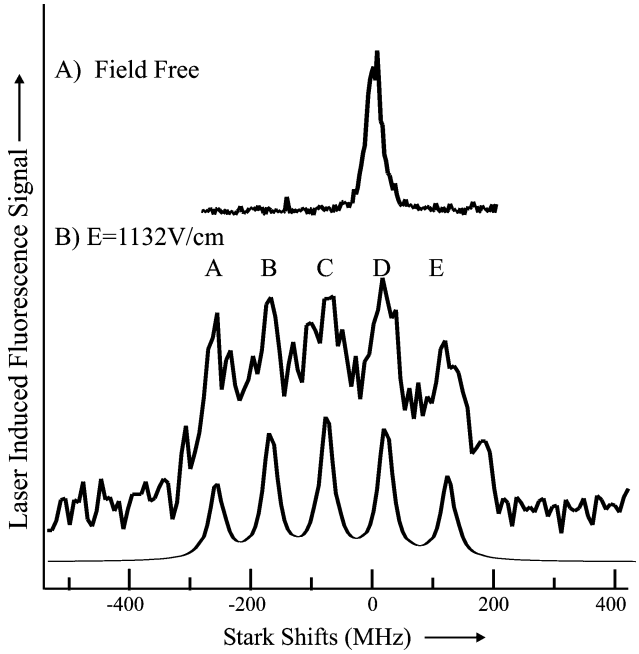

Figure 2. The observed and calculated Stark spectra of the $F'' = 2 \rightarrow F' = 3$ component of the $R(4.5)$ ($\upsilon = 17\,846.438$ cm^{-1}) branch feature recorded at a field strength of 1132 V/cm with parallel polarization.

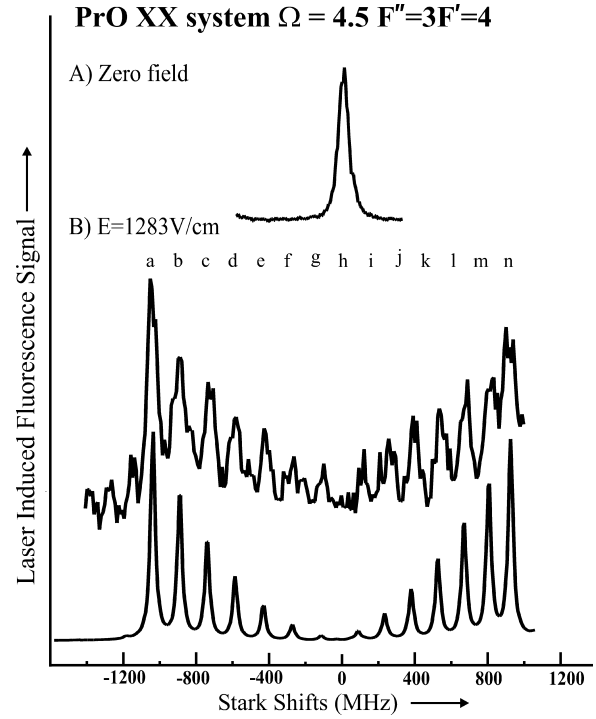

Figure 3. The observed and calculated Stark spectra of the $F'' = 3 \rightarrow F' = 4$ component of the R (4.5) ($\upsilon = 17\,846.360$ cm^{-1}) branch feature recorded at a field strength of 1283 V/cm with perpendicular polarization.

$J'' = 4.5$, $J'' = 6.5$, and $J' = 5.5$ rotational levels obtained by combination/difference of the field-free spectra of the $R(4.5)$ and $P(6.5)$ features are given in Table 1. The values are consistent with, but slightly better determined than, those of ref 2 due to the improved spectral resolution.

b. Stark. Spectra for the $F'' = 2 \rightarrow F' = 3$ ($\upsilon = 17\,846.438$ cm^{-1}) and $F'' = 3 \rightarrow F' = 4$ ($\upsilon = 17\,846.360$ cm^{-1}) magnetic hyperfine components of the $R(4.5)$ line of the XX (0, 0) band with perpendicular and parallel polarization at field strengths ranging from ~1 kV/cm to 2 V/cm were recorded. The observed and calculated Stark spectra of $F'' = 2 \rightarrow F' = 3$ transition recorded at a field strength of 1132 V/cm with parallel polarization are shown in Figure 2. The observed and calculated Stark spectra of $F'' = 3 \rightarrow F' = 4$ transition recorded at a field strength of 1283 V/cm with perpendicular polarization are shown in Figure 3. The assignment of the transitions in Figures 2 and 3 are indicated in the plot of the energy level pattern as a function of applied electric field strength given in Figure 4. Each of the widely spaced hyperfine components of the $J'' = 4.5$ and $J' = 5.5$ rotational levels exist as a very nearly degenerate ($\Delta\nu < 30$ MHz) Λ doublet causing the $F'' = 2 \rightarrow F' = 3$ transition recorded in parallel polarization (Figure 2) to split rapidly into five ($= 2F'' + 1$) components. The centroid of the five features shifts to a lower wavenumber because the $F' = 3$ levels are all pushed to lower energy by second-order Stark mixing with the $F' = 4$ levels. The $F'' = 3 \rightarrow F' = 4$ transition recorded in perpendicular polarization (Figure 3) rapidly splits into two groups of seven ($= 2F'' + 1$) components because of the first-order Stark mixing of the Λ doublet. The lower wavenumber group of seven corresponds to the $\Delta M_F = +1$ transitions, and the upper wavenumber group of seven corresponds to the $\Delta M_F = -1$ transitions. The centroid of the 14 features shifts only slightly to a lower wavenumber because the $F'' = 3$ ($F' = 4$) levels are both pushed to higher and lower energy by second-order Stark mixing with the $F'' = 2$ and $F'' = 4$ ($F' = 3$ and $F' = 5$) levels. The 59 observed shifts and the difference between the calculated and observed Stark shifts are listed in Table 2.

c. Zeeman. The Zeeman splittings in the $F'' = 5 \rightarrow F' = 4$ ($\upsilon = 17\,837.463$ cm^1) and $F'' = 6 \rightarrow F' = 5$ ($\upsilon = 17\,837.417$ cm^{-1}) hyperfine components of the $P(6.5)$ transition were measured. Magnetic fields in the range of 150−240 G were used. The $P(6.5)$ $F'' = 6 \rightarrow F' = 5$ line recorded at a field of

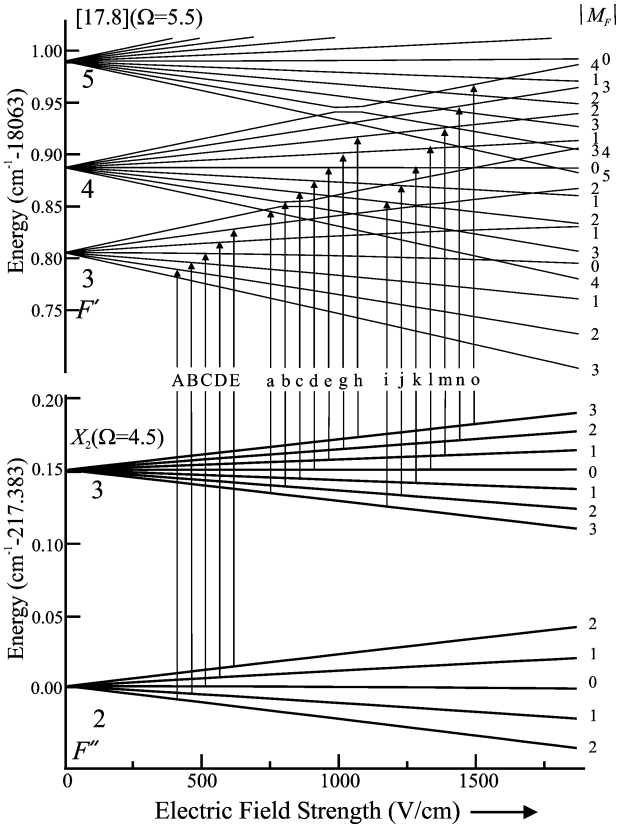

Figure 4. The energy level pattern as a function of applied electric field strength for the levels associated with the $F'' = 3 \rightarrow F' = 4$ and $F'' = 2 \rightarrow F' = 3$ components of the R (4.5) branch. The spectral assignments of Figures 2 and 3 are indicated.

195.9 G for parallel and a field of 264.6 G for perpendicular polarization are given in Figure 5. In parallel polarization, the spectrum consists of 11 ($= 2F' + 1$) components corresponding to $\Delta M_F = 0$. The splitting is symmetric about the field-free transition because the second-order contribution from the adjacent hyperfine levels (e.g., $F' = 4$ and 6; $F'' = 5$ and 7) are negligible due to the small applied field and relatively large field-free spacing (see Table 1). In perpendicular polarization, the $F'' = 6 \rightarrow F' = 5$ line splits into two groups of 11 ($= 2F' + 1$) features, but at 264.6 G, nine of the $\Delta M_F = -1$ transitions overlap with nine of the $\Delta M_F = +1$. A total of 136 magnetic induced shifts were measured and are listed in Table 3, along with the assignment and differences between the observed and predicted shifts.

III. Analysis

In a procedure identical to that of ref 2, the relative energies of the field-free hyperfine components (Table 1) were modeled using the diagonal matrix elements of a phenomenological operator in a nonparity Hund's case c_β ($= |n, \Omega; \Omega JIFM_F\rangle Z$) basis:

$$\langle n'\Omega;\Omega JIFM_F|a_J\hat{I}\cdot\hat{J}|n'\Omega;\Omega JIFM_F\rangle = \frac{1}{2}a[F(F+1) - J(J+1) - I(I+1)] \quad (1)$$

The determined a_J parameters were 0.0510(4) cm^{-1} and 0.0250(2) cm^{-1} for the $J = 4.5$ and 6.5 levels of X_2 ($\Omega = 4.5$) and 0.0204(2) cm^{-1} for the $J = 5.5$ level of the [18.1] ($\Omega = 5.5$) state. The electric field induced splitting and shifts in the R(4.5) line were modeled by numerical diagonalization of a Hund's case c_β matrix representation of $\hat{H}^{Stark} = -\vec{\mu}_{el}\cdot\vec{E}$. The 12 nonparity basis functions associated with $F = 2-7$, $J = 4.5$ of the X_2 ($\Omega'' = 4.5$) state and the 12 nonparity basis functions associated with $F = 3-8$, $J = 5.5$ for the [18.1] ($\Omega = 5.5$) state were used. The values of $\mu_{el}(X_2$ ($\Omega = 4.5$)) and μ_{el}([18.1] ($\Omega = 5.5$)) were optimized by nonlinear least-squares fitting and were determined to be 3.01(6) D and 4.72(5) D for the $\mu_{el}(X_2$ ($\Omega = 4.5$)) and μ_{el}([18.1] ($\Omega = 5.5$)) states, respectively. The numbers in parentheses are the 2σ error estimate. The correlation coefficient was 0.86, and the standard deviation of the fit (= 22 MHz) is commensurate with the measurement uncertainty.

The linear tuning of the energy levels in the applied magnetic field was modeled using the formula expected for the expectation value of $\hat{H}^{Zee} = -\vec{\mu}_m\cdot\vec{B}$ in Hund's case c_β[23]

$$\langle n'\Omega;\Omega JIFM_F|\hat{H}^{Zee}|n'\Omega;\Omega JIFM_F\rangle = g_e\mu_B BM_F\frac{[F(F+1) + J(J+1) - I(I+1)]\Omega}{2J(J+1)F(F+1)} \quad (2)$$

In eq 2, B is the magnetic field strength, g_e is the electronic expectation value of the Zeeman operator, and μ_B is the Bohr magneton. The 136 measured Zeeman shifts of Table 3 were used as input into a linear least-squares fitting routine. The determined g_e values of the X_2 ($\Omega = 4.5$) and [18.1] ($\Omega = 5.5$) states are 4.48(8) and 5.73(6), respectively. The correlation coefficient was 0.96, and the standard deviation of the fit (= 14 MHz) is commensurate with the measurement uncertainty.

Prediction of the relative intensities was very useful in the analysis. In the case of the Stark effect, a 12 × 12 electric dipole transition moment matrix was constructed using the 12 Hund's case c_β basis functions for the [18.1] ($\Omega = 5.5$) and X_2 ($\Omega = 4.5$) states. The transition moment was obtained by cross multiplication of the transition moment matrix by the Hund's case (c_β) eigenvectors. The transition moment was squared and used in conjunction with a Lorentzian line width of 30 MHz full width at half-maximum to predict each spectral feature. In the case of the Zeeman spectral predictions where the field-induced mixing of adjacent hyperfine levels was insignificant, the relative intensities were simply predicted as the square of a three-J symbol;

$$I \propto \left|\begin{pmatrix} F' & 1 & F'' \\ -M_F' & q & M_F'' \end{pmatrix}\right|^2 \quad (3)$$

In eq 3, $q = 0$ or ± 1 for the parallel and perpendicular polarizations.

IV. Discussion

The measurements only determine the magnitude of the permanent electric dipole moment, μ_{el}, but it is expected that the charge distribution is $Pr^{\delta+}O^{\delta-}$ in both the lower and upper states. The values of μ_{el} are much less than a $Pr^{2+}O^{2-}$ pure ionic charge distribution would suggest, primarily due to the polarization of the 6s orbital. The X_2 ($\Omega = 4.5$) ($E = 220$ cm^{-1}) state differs from the X_1 ($\Omega = 3.5$) ($E = 0$ cm^{-1}) state only in the orientation of the spin of the 6s electron (vide infra), and it is expected that μ_{el} for the X_1 ($\Omega'' = 3.5$) ($E = 0$ cm^{-1}) state will be very similar to the 3.01(6) D value measured here for the X_2 ($\Omega = 4.5$) ($E = 220$ cm^{-1}) state. The measured μ_{el} (X_2 ($\Omega = 4.5$)) value is much less than the predicted ground-state values of 3.86 D[10] and 4.114 D,[11] presumably because neither calculation accurately accounts for the polarization of the 6s orbital. The large increase in μ_{el} upon electronic excitation and (3.01(6) D → 4.72(5) D) is not due to an increase in bond length, but rather, a change in electronic character. Evidently, the electronic

TABLE 2: Observed and Calculated Stark Shifts for the XX (0,0) Band of PrO

field					shift (MHz)		field					shift (MHz)	
branch	F''	(V/cm)	M_F'	M_F''	obs.	dif	branch	F''	(V/cm)	M_F'	M_F''	obs	dif
R(4.5)	2	981	–2	–2	–207	14	⊥	3	981	0	–1	304	–8
∥			–1	–1	–138	5				1	0	392	–25
			0	0	–71	–9				2	1	499	–22
			1	1	22	–1				3	2	592	–29
			2	2	111	–3				4	3	695	–20
		1132	–2	–2	–266	–3		3	1132	–4	–3	–846	33
			–1	–1	–167	7				–3	–2	–731	24
			0	0	–74	8				–2	–1	–597	31
			1	1	19	4				–1	0	–482	18
			2	2	122	3				0	1	–362	8
		1509	–2	–2	–362	9				1	2	–227	10
			–1	–1	–248	11				0	–1	358	–1
			0	0	–132	10				1	0	492	10
			1	1	–8	11				2	1	617	15
			2	2	114	–1				3	2	737	21
		1887	–2	–2	–458	29				4	3	790	–30
			–1	–1	–332	21			1283	–4	–3	–1040	–40
			0	0	–202	15				–3	–2	–902	–42
			1	1	–72	0				–2	–1	–715	–53
			2	2	91	5				–1	0	–575	–6
										0	1	–418	3
⊥	3	981	–4	–3	–727	32				1	2	–283	–14
			–3	–2	–615	36				2	3	–103	13
			–2	–1	–507	35				–2	–3	129	54
			–1	0	–339	32				–1	–2	292	25
			0	1	–297	22				0	–1	419	13
			1	2	–184	22				1	0	566	21
			2	3	–82	11				2	1	706	24
			–2	–3	79	–1				3	2	841	30
			–1	–2	192	–14				4	3	943	21

rms = 22 MHz

excitation is a promotion of the 6s electron to a much less polarizable, metal-centered, orbital.

The quasi-atomic picture established from a LFT model of the $Pr^{2+}O^{2-}$ ionic bonding can be used for the interpretation of the g_e-factors. The LFT predictions for PrO[4–9] as well as the semiempirical valence electron method[12] and density functional theory[11] predictions demonstrated that although the $4f^3$ configuration is most stable for Pr(III), the $4f^26s$ configuration is stabilized in the presence of the O^{2-} and dominates in the description of the low-lying states of PrO. The $4f^26s$ atomic configuration gives rise to ^{4}H, ^{2}H, ^{4}F, ^{2}F, ^{2}G, ^{2}D, ^{2}I, ^{4}P, ^{2}P, and ^{2}S terms, listed in order of increasing energy. Only the $^4H-^2H$ pair of terms is relevant to the discussion of the low-lying ($E <$ 6000 cm^{-1}) electronic states of PrO. The term splitting of the $^4H-^2H$ states is small compared to the spin−orbit splitting because the G^3(sf) exchange integral is small owing to the large disparity in radial extent of the 6s and 4f orbitals. Therefore, the levels of the $^4H-^2H$ pair of terms exhibit an energy pattern that is more readily described in a *Jj*-coupling scheme in which the electrons of the 4f core are Russell−Saunders-coupled and characterized by the approximately good quantum numbers L_c, S_c, and J_c. The core total angular momentum, J_c, then couples with the peripheral 6s electron to give the total atomic electronic angular momentum, J_a:

$$\Psi^{el}(\mathrm{Pr(III)} \approx \left|\left((S_cL_c)J_c(4f^2)\right)6s\left(s=\frac{1}{2}\right)J_a, M_{J_a}\right\rangle = \left|J_c, J_a, M_{J_a}\right\rangle \quad (4)$$

The low-energy level pattern for Pr(III) is predicted to consist of three pairs of closely spaced electronic states associated with $J_c = 4$, 5, and 6 of a ^{3}H(f^2) term, which is loosely coupled to the 6s electron to produce $J_a = J_c \pm 1/2$. The cylindrically symmetric electric field along the molecular axis due to O^{2-} lifts the M_{J_a} degeneracy, and the lowest 33 Hund's case (c), $|nJ\Omega\rangle$, electronic states of PrO correlate to the six Pr(III) electronic states arising from coupling the 6s electron with the $^3H_{Jc=4,5,6}(4f^2)$ levels. The molecular states can be arranged into

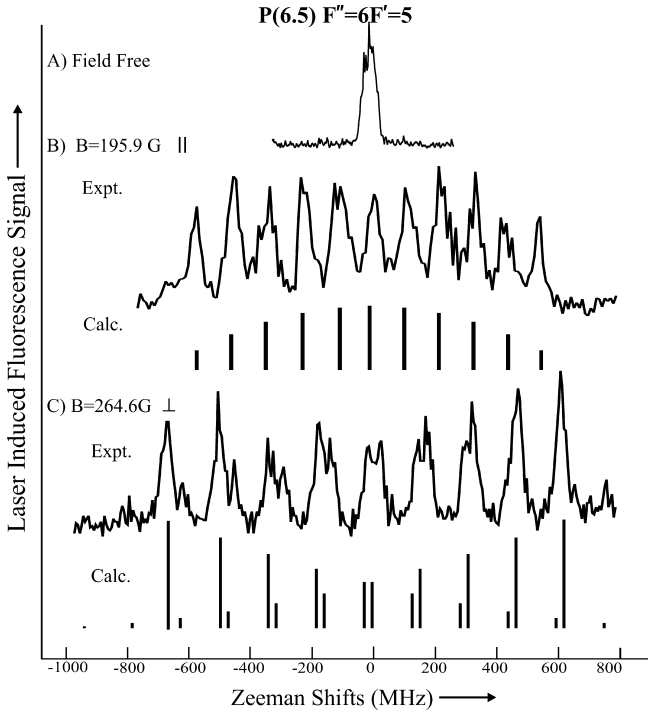

Figure 5. The $P(6.5)$ $F'' = 6 \rightarrow F' = 5$ line recorded field-free (top), at a field of 195.9 G for parallel polarization (middle), and a field of 264.6 G for perpendicular polarization (bottom) along with predicted transitions.

TABLE 3: Observed and Calculated Zeeman Shifts for the XX(0, 0) Band System of PrO

					shift (MHz)								shift (MHz)	
branch	F''	field[a]	M_F'	M_F''	obs	dif[b]	branch	F''	field[a]	M_F'	M_F''	obs	dif[b]
$P(6.5)$	5	150.4	4	4	–430	36	$P(6.5)$	6	150.4	–1	0	185	9
∥			3	3	–333	17	⊥			–2	–1	303	35
			2	2	–228	5				–3	–2	374	15
			1	1	–111	6				3	2	–370	–11
			0	0	–14	–14				2	1	–258	10
			–1	–1	106	–11				1	0	–178	–2
			–2	–2	233	0				0	–1	–81	4
			–3	–3	354	4				–1	–2	23	16
			–4	–4	448	–19				–2	–3	106	8
		195.9	4	4	–600	7				–3	–4	185	–4
			3	3	–454	2				–4	–5	303	23
			2	2	–304	0				–5	–6	374	2
			1	1	–155	–3			240.5	5	6	–618	–24
			0	0	–13	–13				4	5	–470	–21
			–1	–1	136	–16				3	4	–325	–23
			–2	–2	315	11				2	3	–169	–12
			–3	–3	461	5				1	2	–15	–5
			–4	–4	586	–22				0	1	105	–31
	6	150.4	5	5	–451	6				–1	0	289	7
			4	4	–363	3				–2	–1	448	19
			3	3	–275	–1				–3	–2	563	–12
			2	2	–185	–3				3	2	–570	5
			1	1	–97	–5				2	1	–422	7
			0	0	0	0				1	0	–268	14
			–1	–1	89	–3				0	–1	–153	–17
			–2	–2	167	–16				–1	–2	14	4
			–3	–3	259	–15				–2	–3	148	–8
			–4	–4	349	–16				–3	–4	293	–10
			–5	–5	422	–35				–4	–5	435	–13
		195.9	5	5	–599	–3				–5	–6	582	–13
			4	4	–467	9			264.6	5	6	–678	–24
			3	3	–355	2				4	5	–500	–7
			2	2	–227	11				3	4	–327	6
			1	1	–101	18				2	3	–162	10
			0	0	15	15				1	2	–2	9
			–1	–1	125	6				0	1	161	11
			–2	–2	246	8				–1	0	320	9
			–3	–3	353	–5				–2	–1	480	8
			–4	–4	455	–22				–3	–2	642	10
			–5	–5	570	–25				–4	–3	796	3
		240.5	5	5	–749	–18				5	4	–941	12
			4	4	–595	–11				4	3	–811	–18
			3	3	–425	13				3	2	–631	1
			2	2	–288	4				2	1	–459	12
			1	1	–138	8				1	0	–294	17
			0	0	15	15				0	–1	–150	0
			–1	–1	163	16				–1	–2	16	5
			–2	–2	305	12				–2	–3	176	4
			–3	–3	434	–4				–3	–4	336	3
			–4	–4	584	–1				–4	–5	493	0
			–5	–5	755	25				–5	–6	642	–12
⊥	6	150.4	5	6	–370	1	$R(4.5)$	2	122.7	1	0	–239	7
			4	5	–258	23	⊥			–1	0	239	–7
			3	4	–178	11			155.0	1	0	–316	–5
			2	3	–81	16				–1	0	316	5
			1	2	23	29							
			0	1	106	21				rms = 14 MHz			

[a] Gauss. [b] Difference = observed − calculated.

stacks of levels from $|\Omega| = = J_a, J - 1, ..., J_a - 6$. The X_i, W_i, V_i, U_i, and T_i, labeling of the states of PrO corresponds to the approximately good quantum number $|\Omega| = J_a, J_a - 1, J_a - 2, J_a - 3$, and $J_a - 4$, respectively. The subscript i identifies each state in the stack of levels with constant $J_a - |\Omega|$ (ref 24). To the first approximation, the electronic wave functions for the X_1 ($\Omega = 3.5$) and X_2 ($\Omega = 4.5$) states of PrO are simply the Pr(III) atomic functions $|J_c = 4; J_a = 4.5, M_{J_a} = \pm 4.5\rangle$ and $|J_c = 4, J_a = 3.5, M_{J_a} = \pm 3.5\rangle$, respectively. The O^{2-} induced electrostatic potential and the spin−orbit coupling mixes the Pr(III) basis functions. Carette et al.[7] used a zero adjustable parameter LFT to predict that the electrostatic and spin−orbit mixing produces

$$\Psi^{el}(X_1\ (\Omega = 3.5)) = 0.93 \times |4, 3.5\rangle - 0.30 \times |4, 4.5\rangle + 0.18 \times |5, 4.5\rangle \quad (5)$$

and

$$\Psi^{el}(X_2\ (\Omega = 4.5)) = 0.98 \times |4, 4.5\rangle - 0.20 \times |5, 5.5\rangle - 0.06 \times |5, 4.5\rangle \quad (6)$$

The semiempirical valence-electron calculation[12] predicted that Ψ^{el} (X_2 ($\Omega = 4.5$)) is composed of 57% of $|4, 4.5\rangle$ and 45% of

$|5, 5.5\rangle$. It is reasonable to expect that the remaining 8% of the wavefuction is $|5, 4.5\rangle$.

The predicted wavefuctions can be used to calculate the expectation of the Zeeman operator from which the theoretical g_e-factors for the nonrotating molecule are obtained. The g_e-factors are simply the expectation values of $\hat{H}^{Zeeman}$ over the electronic wave function, Ψ^{el}. The Zeeman Hamiltonian operator is

$$\hat{\mathbf{H}}^{\text{Zeeman}} = -\vec{\mu}_m \cdot \vec{B} = \mu_B T^1(B) \cdot \left[\sum_i g_l T^1(l_i) + g_s T^1(s_i) \right] \quad (7)$$

where μ_B is the Bohr magneton, B is the magnetic flux in Gauss, and g_l and g_s are the electronic orbital and spin g_e-factors. The explicit formula for the expectation value of $\hat{\mathbf{H}}^{Zeeman}$ when Ψ^{el} is expressed in the Jj-coupled basis functions (eq 4) is[25]

$$g_e((L_C,S_C)'J_C;(l's)j;J_a\Omega) = (A + B)\frac{\Omega}{4J_a(J_a + 1)} \quad (8)$$

where

$$A = \frac{[J_a(J_a + 1)J_c(J_c + 1) - j(j + 1)]}{J_c(J_c + 1)}[3J_c(J_c + 1) + S_c(S_c + 1) - L_c(L_c + 1)] \quad (9)$$

and

$$B = \frac{[J_a(J_a + 1) + j(j + 1) - J_c(J_c + 1)]}{j(j + 1)}[3j(j + 1) + s(s + 1) - l(l + 1)] \quad (10)$$

The g_e-factor for the $|4, 4.5\rangle$, $|5, 5.5\rangle$ and $|5, 4.5\rangle$ basis functions are 4.20, 5.05, and 4.25, respectively. Using the LFT predicted coefficients of eq 6, the g_e-factor for the X_2 ($\Omega = 4.5$) ($E = 220$ cm^{-1}) state is predicted to be 4.25, which is slightly less than the experimental value of 4.48(8), suggesting there should be a larger coefficient for the $|5, 5.5\rangle$ basis function. The semiempirical valence-electron predicted wave function[12] for the X_2 ($\Omega = 4.5$) ($E = 220$ cm^{-1}) state gives a g_e-factor of 4.50, if it is assumed that the unspecified 8% composition is $|5, 4.5\rangle$.

V. Concluding remarks

The published predictions for μ_{el} are in poor agreement with the presently determined value. The determined μ_{el} (X_2 ($\Omega = 4.5$)) of PrO is consistent with, but slightly lower than ($\sim$0.15 D), the monotonic atomic number dependence observed for the ground state μ_{el} values of other lanthanide monoxide molecules: LaO (3.207 D),[13] CeO (3.119D) (see accompanying article), PrO (3.01 D) (this work), NdO (3.369D),[14] SmO (3.52 D),[15] DyO (4.51 D),[16] HoO (4.80 D),[17] and YbO (5.89 D).[18] Given that the ground state μ_{el} value for UO (= 3.363 D)[26] is nearly identical to that of isovalent NdO, it may be expected that the above dipole moment can be used to predict the μ_{el} values for the isovalent actinide monoxides, which are much more difficult to measure experimentally.

A comparison of predicted and observed g_e values for the X_2 ($\Omega = 4.5$) state strongly suggests that (a) the calculated LFT quasi-atomic wave function of Carette et al.[7] underestimates the mixing between the $|J_c = 4, J_a = 4.5\rangle$ and $|J_c = 5, J_a = 5.5\rangle$ atomic basis states and (b) the wave function obtained from the semiempirical valence-electron calculations of Kotzian et al.[12] more accurately account for this configurational mixing. Childs et al.[9] and the Field group[4] have demonstrated that LFT wave functions can be used for a quantitative prediction of magnetic hyperfine interactions. Here, we have demonstrated that g_e-factors, which are readily extracted from optical Zeeman spectroscopy, are a complementary powerful diagnostic tool for testing the various models for calculating Ψ^{el}. Unlike many other parameters extracted from spectroscopic analyses (e.g., rotational constant), it is expected that the nonadiabatic contributions to g_e are not severe. Like the case of μ_{el}, the availability of theoretical predicted g_e-factors would foster a synergism between theory and experiment.

Acknowledgment. This work has been supported by grants from the Fundamental Interactions Branch, Division of Chemical Sciences, Office of Basic Energy Sciences, Department of Energy (DE-FG02-01ER15153-A003) and by the Natural Sciences and Engineering Research Council (NSERC) of Canada. The authors thank Dr. Jinhai Chen for assistance with the Stark measurements.

References and Notes

(1) Dulick, M.; Field, R. W.; Beaufils, J. Cl. *J. Mol. Spectrosc.* **1979**, *78*, 333.
(2) Dulick, M.; Field, R. W.; Beaufils, J. Cl. *J. Mol. Spectrosc.* **1981**, *87*, 268.
(3) Dulick, M.; Field, R. W.; Beaufils, J. Cl.; Schamps, J. *J. Mol. Spectrosc.* **1981**, *87*, 278.
(4) Dulick, M.; Field, R. W. *J. Mol. Spectrosc.* **1985**, *113*, 105.
(5) Field, R. W. *Bunsen−Ges. Ber. Phys. Chem., Ber.* **1982**, *86*, 771.
(6) Dulick, M.; Murad, E.; Barrow, R. F. *J. Chem. Phys.* **1986**, *85*, 385.
(7) Carette, P.; Hocquet, A. *J. Mol. Spectrosc.* **1988**, *131*, 301.
(8) Kaledin, L. A.; McCord, J. E.; Heaven, M. C. *J. Mol. Spectrosc.* **1993**, *158*, 40.
(9) Childs, W. J.; Azuma, Y.; Goodman, G. L. *J. Mol. Spectrosc.* **1990**, *144*, 70.
(10) Dolg, M.; Stoll, H. *Theor. Chim. Acta* **1989**, *75*, 369.
(11) Wu, Z.; Guan, W.; Meng, J.; Su, Z. *J. Cluster Sci.* **2007**, *18*, 444.
(12) Kotzian, M.; Rösch, N. *J. Mol. Spectrosc.* **1991**, *147*, 346.
(13) Suenram, R. D.; Lovas, F. J.; Fraser, G. T.; Matsumura, K. *J. Chem. Phys.* **1990**, *92*, 4724.
(14) Linton, C.; Ma, T.; Wang, H.; Steimle, T. C. *J. Chem. Phys.* **2008**, *129*, 124310.
(15) Linton, C.; James, A. M.; Simard, B. *J. Chem. Phys.* **1993**, *99*, 9420.
(16) Linton, C.; Simard, B. *J. Chem. Phys.* **1992**, *96*, 1698.
(17) Chen, J.; Steimle, T. C.; Linton, C. *J. Mol. Spectrosc.* **2005**, *232*, 105.
(18) Steimle, T. C.; Goodridge, D. M.; Linton, C. *J. Chem. Phys.* **1997**, *107*, 3723.
(19) Steimle, T. C. *Int. Rev. Phys. Chem.* **2000**, *19*, 455.
(20) Virgo, W. L.; Steimle, T. C.; Brown, J. M. *Astrophys. J.* **2005**, *628*, 567.
(21) IODINESPEC4; Toptica Photonics: Munich, Germany; www.toptica.com.
(22) Schawlow, A. L. *Rev. Mod. Phys.* **1982**, *54*, 697.
(23) Brown, J. M.; Carrington, A. *Rotational Spectroscopy of Diatomic Molecules*; Cambridge University Press: Cambridge, 2003.
(24) Linton, C.; Dulick, M.; Field, R. W.; Carette, P.; Leyland, P. C.; Barrow, R. F. *J. Mol. Spectrosc.* **1983**, *102*, 441.
(25) Schall, H.; Gray, J. A.; Dulick, M.; Field, R. W. *J. Chem. Phys.* **1986**, *85*, 751.
(26) Heaven, M. C.; Goncharov, V.; Steimle, T. C.; Ma, T.; Linton, C. *J. Chem. Phys.* **2006**, *125*, 204314.

JP900677G